Journal of Power Sources 195 (2010) 69–78

Contents lists available at ScienceDirect

Journal of Power Sources

journal homepage: www.elsevier.com/locate/jpowsour

Modelling of tubular-designed solid oxide fuel cell with indirect internal reforming operation fed by different primary fuels

P. Dokmaingam[a], S. Assabumrungrat[b], A. Soottitantawat[b], N. Laosiripojana[a,*]

[a] The Joint Graduate School of Energy and Environment, King Mongkut's University of Technology Thonburi, 126 Prachauthit Rd., Bangmod, Tungkru, Bangkok 10140, Thailand
[b] Department of Chemical Engineering, Faculty of Engineering, Chulalongkorn University, Bangkok 10330, Thailand

ARTICLE INFO

Article history:
Received 25 March 2009
Received in revised form 10 June 2009
Accepted 23 June 2009
Available online 10 July 2009

Keywords:
Indirect internal reforming
Solid oxide fuel cell
Methane
Methanol
Ethanol
Biogas

ABSTRACT

Mathematical models of an indirect internal reforming solid oxide fuel cell (IIR-SOFC) fed by four different primary fuels, i.e., methane, biogas, methanol and ethanol, are developed based on steady-state, heterogeneous, two-dimensional and tubular-design SOFC models. The effect of fuel type on the thermal coupling between internal endothermic reforming with exothermic electrochemical reactions and system performance are determined. The simulation reveals that an IIR-SOFC fuelled by methanol provides the smoothest temperature gradient with high electrochemical efficiency. Furthermore, the content of CO_2 in biogas plays an important role on system performance since electrical efficiency is improved by the removal of some CO_2 from biogas but a larger temperature gradient is expected.

Sensitivity analysis of three parameters, namely, a operating pressure, inlet steam to carbon (S:C) ratio and flow direction is then performed. By increasing the operating pressure up to 10 bar, the system efficiency increases and the temperature gradient can be minimized. The use of a high inlet S:C ratio reduces the cooling spot at the entrance of reformer channel but the electrical efficiency is considerably decreased. An IIR-SOFC with a counter-flow pattern (as based case) is compared with that with co-flow pattern (co-flow of air and fuel streams through fuel cell). The IIR-SOFC with co-flow pattern provides higher voltage and a smoother temperature gradient along the system due to superior matching between heat supplied from electrochemical reaction and heat required for steam reforming reaction; thus it is expected to be a better option for practical applications.

1. Introduction

During the past two decades, several types of fuel cell have been continuously developed and modified. Among them, the solid oxide fuel cell (SOFC) has attracted much interest for stationary power generation since it provides high efficiency with low pollutant emission [1]. Generally, SOFC is operated at high temperatures (1073–1473 K), thus hydrocarbon fuels (e.g., methane) can be applied as a primary fuel when the system is operated with internal reforming (IR-SOFC). This operation uses the heat generated from the exothermic electrochemical reaction to conduct the endothermic (steam) reforming of hydrocarbons [2–5].

Theoretically, there are two main designs of a IR-SOFC namely, direct internal reforming (DIR-SOFC) and indirect internal reforming (IIR-SOFC). In the DIR-SOFC approach, together with electrochemical reaction, the reforming reaction occurs simultaneously at the anode side of SOFC. Thus, a high heat transfer rate can be achieved from this operation; nevertheless, the anode material must be optimized for both reactions and can be easily poisoned by deposition of carbon produced from the reforming of hydrocarbons. In an IIR-SOFC, the endothermic reforming reaction takes place at a reformer, which is in close thermal contact with the anode side of the SOFC where exothermic electrochemical reaction occurs. The great advantage of an IIR-SOFC is that the released heat can be utilized efficiently and the anode material is not subject to coke deposition occurring from the cracking and reforming of hydrocarbons, thus the primary fuels for IIR-SOFC are more flexible than DIR-SOFC. It is noted that the main drawback of IIR-SOFC is the mismatch between the rates of endothermic and exothermic reactions. This problem leads to significant local temperature reduction, particularly near the entrance of the internal reformer [3,4,6], which can result in mechanical failure due to thermally induced stresses. Importantly, the temperature gradient along the SOFC system is affected by several operating parameters, namely, inlet temperature, pressure and drawn current [4,6], as well as the type of primary inlet fuel.

Focusing on the primary fuel selection, methane (or natural gas) is accepted to be the most applicable fuel for IR-SOFC due to its abundance and well-developed supply infrastructure. Among other

* Corresponding author. Tel.: +66 2 4708309; fax: +66 2 8726736.
E-mail address: navadol_l@jgsee.kmutt.ac.th (N. Laosiripojana).

0378-7753/$ – see front matter © 2009 Elsevier B.V. All rights reserved.
doi:10.1016/j.jpowsour.2009.06.102

Nomenclature

A_{act}	area (m^2)
A_{act}	active area $= \frac{\pi(d_r - 2\Gamma_{cat})L}{\pi(d_r^2 - (d_r - 2\Gamma_{cat})^2 L)}$ (m^2)
C_P	specific heat of the gas streams ($kJ\,mol^{-1}\,K^{-1}$)
c_i	concentration of component i ($mol\,m^{-3}$)
$D_{i,j}$	binary diffusion of component i and j ($m^2\,s^{-1}$)
$D^e_{i,mix}$	effective molecular diffusivity ($m^2\,s^{-1}$)
d	diameter (m)
Eff	efficiency
F	Faraday's constant ($96{,}484\,C\,mol^{-1}$)
$F_{r,s}$	gray-body transfer factor from reformer surface to solid oxide surface
ΔH	heat of reaction ($kJ\,mol^{-1}$)
J_0	Exchange current density ($A\,m^{-2}$)
J	current density ($A\,m^{-2}$)
k_p	permeability
LHV_i	lower heating value of component i
M_i	molecular weight of component i ($kg\,kJ^{-1}$)
n_i	number of mole of component i
p^0	standard partial pressure (Pa)
p_i	partial pressure of species i
P_{SOFC}	power density ($W\,m^{-2}$)
Q_{elec}	local generated heat ($W\,m^{-2}$)
R_k	rate of reaction k
R_g	universal gas constant: $8.414\,kJ\,mol^{-1}\,K^{-1}$.
R_{ohm}	ohmic resistant ($k\Omega\,m^{-2}$)
T	temperature (K)
$\vec{v}$	fluid velocity ($m\,s^{-1}$)
y_i	the mole fraction of gas

Greek letters

ρ	density ($kg\,m^{-3}$)
ε_m	emittance
$\tilde{\mu}$	effect of viscosity (Pa s)
γ	special Fuller et al. diffusion volume [13]
$\alpha_{a,c}$	charge transfer coefficient of anode and cathode
σ	Stefan–Boltzmann coefficient
ε	porosity
τ	tortuosity
λ	thermal conductivity ($kJ\,m^{-1}\,s^{-1}K^{-1}$)
η	voltage drop (V)
Γ	thickness (m)

Subscripts

a	air channel
i	component (methane, water, hydrogen, etc.)
j	reaction (SRM, WGS, etc.)
f	fuel channel
p	particle
r	reformer
s	solid oxide fuel cell
Act	activation losses
Cat	catalyst
Cell	cell stack
Con	concentration losses
Elec	electrical
Thermal	thermal

potential primary fuels, ethanol and methanol are also interesting candidates due to their ready availability, high specific energy, sulfur-free content and storage transportation convenience [5]; moreover, they can be produced renewably from both chemical and biological processes. In addition to these three types of fuel, biogas is another attractive candidate—particularly for agricultural countries since it is a promising renewable fuel that can be produced biologically from the waste residues. Normally, after desulfurization, biogas is composed of approximately 60–65 vol.% of methane and 35–40 vol.% of CO_2.

In the present study, a set of mathematical models has been developed to predict and compare the behaviour of a tubular IIR-SOFC fuelled by methane, methanol, ethanol, and biogas. The models are coded in the COMSOL® program within 2D axisymmetric application. From the simulation, the performance of an IIR-SOFC (i.e., electrical efficiency and temperature gradient along the system) fuelled by these four types of primary fuels are determined; in addition, the effects of inlet steam to carbon (S:C) ratio, operating pressure and gas flow patterns on the performance of the IIR-SOFC are also investigated. Finally, a suitable type of primary fuel and suitable operating conditions for an IIR-SOFC system are identified.

2. Mathematical models

2.1. Kinetic equations for steam reforming of primary fuels

A steam reforming reaction was chosen to convert methane, methanol, ethanol and biogas to hydrogen-rich gas. The kinetic equations for each reaction were based on previous reports in the literature [7–10]. For methane reforming, the well-known kinetic models and reaction mechanisms proposed by Xu and Froment [7] were applied. For methanol reforming, the rate expressions reported by Peppley et al. [8] were selected, whereas the simulation of ethanol reforming was based on the rate expressions proposed by Sahoo et al. [10]. For biogas, the rate expressions of methane steam reforming with coupling of carbon dioxide reforming reported by Abashar [9] were applied.

2.2. Model geometry and assumptions

A tubular-designed IIR-SOFC was selected, as shown schematically in Fig. 1. According to this configuration, primary fuels (e.g., methane, methanol, ethanol, or biogas) and steam are converted to hydrogen-rich gas in an internal catalytic packed-bed reformer before being introduced to the fuel channel of the SOFC. Simultaneously, air is fed in an opposite flow direction through the air channel. It is noted that all dimensions and physical properties of SOFC system in the present work, which are summarized in Table 1, are based on the work of Aguiar et al. [4].

The mathematical model was developed as the smallest, single, unit cell taking into account the effect of temperature on gas distribution, reactant conversion and charge transfer. Two main sets of equations, namely, for the internal reformer and the SOFC stack (including electrodes and solid electrolyte) were applied to predict the concentration and temperature gradients along the system based on the following assumptions:

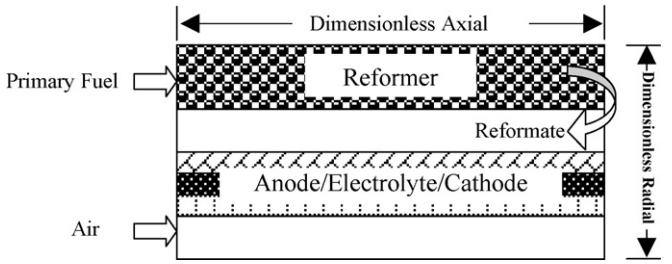

Fig. 1. Schematic diagram of tubular-designed SOFC with indirect internal reforming operation.

Table 1
Dimensional parameter for modelling.

Parameters	Value
Reformer diameter	0.6 cm
Gap between reformer to fuel channel	0.24 cm
Anode thickness	0.07 cm
Electrolyte thickness	20 μm
Cathode thickness	50 μm
Gap between cathode to air channel	0.3 cm
Length	60 cm
Anode	
Porosity (ε)	0.35
Tortuosity (τ)	4.80
Pore radius (r_p)	0.20 μm
Particle diameter (dp)	1.00 μm
Cathode	
Porosity (ε)	0.35
Tortuosity (τ)	4.00
Pore radius (r_p)	0.25 μm
Particle diameter (dp)	1.25 μm

- Each section is considered to be under non-isothermal, steady-state conditions.
- Ideal gas behaviour is applied for all gas components.
- Diffusion in the gas phase and pressure drop in the SOFC stack and reformer are ignored.
- The operating cell potential is constant along the cell coordinate.
- Final fuel utilization is fixed constantly at 80%.

By adopting a non-isothermal state, the calculated gas properties are derived as the function of temperature; thus, momentum, mass and energy balances are integrated under the conditions of interest. According to the tubular IIR-SOFC design (as shown in Fig. 1), the system structure consists of two main parts, i.e., porous and bulk gas channels. The transport behaviour of both parts is treated differently, as explained in the following sections.

2.2.1. Gas transport

Gas transport behaviour in the porous media, reformer and cell layer was calculated by means of the Brinkmen equation (Eq. (1)), whereas the Navier–Stokes equation (Eq. (2)) was applied to predict the momentum transfer in gas channels [11].

$$\nabla p = -\frac{\mu}{k_p}v + \tilde{\mu}\nabla^2 v \tag{1}$$

$$v\,\nabla(\rho v) = -\nabla p + \tilde{\mu}\nabla^2 v \tag{2}$$

where v is the fluid velocity; ρ is the density (kg m^{-3}); p is the pressure (Pa); $\tilde{\mu}$ is the effect of viscosity (as function of temperature), and k_p is the permeability. In this system, the diffusion properties of several gas species were investigated by using the binary diffusion flux, as given by [12]:

$$D_{i,j} = \frac{(0.00143)T^{1.75}}{pM_{i,j}^{1/2}[\gamma_i^{1/3} + \gamma_j^{1/3}]} \tag{3}$$

where $D_{i,j}$ is the binary diffusion of component i (mol m^{-1} s^{-1}); T is the temperature (K); p is the pressure (Pa); $M_{i,j} = 2/(1/M_i + 1/M_j)$; M_i is the molecular weight of component i; γ is a special diffusion volume (reported by Fuller et al. [13]); p_i is the partial pressure of component i. In the case of transportation through porous media, the diffusion behaviour is corrected by taking into account the porosity, ε, and the tortuosity, τ, namely, the effective diffusivity coefficiency (m^2 s^{-1}), $D^e_{i,mix}$:

$$D^e_{i,mix} = \frac{\varepsilon}{\tau}\sum D_{i,j} \tag{4}$$

Generally, gas diffusion through electrode layers can be explained by the coupling of two diffusion mechanisms, namely, molecular and Knudsen diffusions. This is known as the dusty gas model (DGM) [14]. If the mean free path of gas molecular species is larger than the pore diameter, Knudsen diffusion is the main mechanism; otherwise, molecular diffusion will dominate.

2.2.2. Ionic transport

The electricity generation was calculated from the relation between polarization and the activated area of SOFC. Activation, concentration and ohmic polarization are known as major losses for high-temperature fuel cells like SOFCs. Activation loss arises from an activation barrier to the electrochemical reaction at the electrode. In this work, the activation polarization, η_{act}, was computed by [15]:

$$J_i = J_0\left[\exp\left(\frac{\alpha_a F\eta_{act}}{R_g T}\right) - \exp\left(\frac{-(1-\alpha_c)F\eta_{act}}{R_g T}\right)\right] \tag{5}$$

where J_i is the current density (A m^{-2}); J_0 is the exchange current density (A m^{-2}); R_g is the universal gas constant (kJ mol^{-1} K^{-1}); F is the Faraday constant. All relevant parameters were reported by Zhu et al. [16]. The concentration polarization occurs due to the resistance to gas diffusion through the porous media. Generally, gas diffusion behaviour can be predicted by three mathematical models: Fick's model, Dusty gas model (DGM), and Stefan–Maxwell model; the DGM was chosen in the present work. Ohmic polarization arises from the ion transport across the cell, which mainly depends on the ionic conductivity of the SOFC material. By applying ohm's law, the relation of ohmic polarization and material resistivity can be determined. It is noted that, in the present work, the material properties reported by Zhu et al. [16] were used. This voltage drop was computed by the simplified equation:

$$\eta_{ohmic} = J.R_{ohm} \tag{6}$$

where η_{ohmic} is the voltage drop caused by ohmic losses (V); J is the current density (A m^{-2}), and R_{ohm} is the ohmic resistant per unit area (kΩ m^2). It is noted that although both H_2 and CO can be electrochemically consumed in a SOFC, it has been reported that the

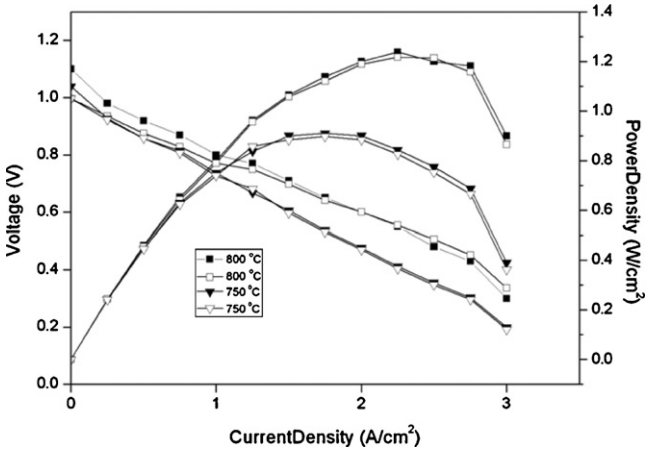

Fig. 2. I–V curve validation between simulation results of present work (blank symbols) with those from Lin et al. [16] (solid symbols).

Table 2
Thermal properties of each fuel under isothermal condition (1173 K and 1 bar).

Fuel	Thermal properties	
	LHV	Thermal efficiency (%)
Methane	744.7	49.4
Biogas	466.8	39.5
Methanol	631.5	76.3
Ethanol	1194.3	69.7

rate of electricity generation from CO is three times lower than that of H_2 [17]; thus the rate of CO oxidation in SOFC has been neglected in this study. At the anode|electrolyte interface, H_2 is electrochemically oxidized whereas O_2 is consumed at the cathode|electrolyte interface. The conversion rate of H_2, R_{elec,H_2}, and O_2, R_{elec,O_2}, at the indicated boundary was simulated from Eqs. (7) and (8), respectively:

$$R_{elec,H_2} = \frac{J_{H_2}}{2F} \tag{7}$$

$$R_{elec,O_2} = \frac{J_{O_2}}{4F} \tag{8}$$

The reliability of these electrochemical equations, coded in COMSOL® program, was validated by comparison with the results from the work of Lin et al. [18], as shown in Fig. 2. Clearly, the results are in good agreement.

2.2.3. Heat transfer

Conduction heat transfer along stack materials, convection heat transfer from fluid flow though the system and radiation between the reformer and the solid electrolyte were considered to predict the temperature distribution of the IIR-SOFC system. In the bulk gas channel, both conduction and convection heat transfer were calculated by:

$$\nabla \cdot (v\rho c_p T) - \nabla \cdot (\lambda \cdot \nabla T) = 0 \tag{9}$$

where v is the fluid velocity ($m\,s^{-1}$); ρ is the gas density ($kg\,m^{-3}$); c_p is the specific heat ($kJ\,kg^{-1}\,K^{-1}$); λ is the thermal conductivity ($kJ\,m^{-1}\,s^{-1}\,K^{-1}$); T is the temperature (K). It is noted that the influence of the radiation between the reformer and the solid electrolyte was also taken into account by considering the heat required for steam reforming in the reformer (Eq. (10)) and the heat of electrochemical reaction at the anode|electrolyte layer (Eq. (11)) [19].

$$\nabla \cdot (v\rho c_p T) - \nabla \cdot (\lambda \cdot \nabla T) + (-\Delta H_{reform}) R_{reform} + \frac{\sigma(T_r^4 - T_s^4)}{(1-\varepsilon_m/\varepsilon_m A)_r + 1/A_r F_{r,s} + (1-\varepsilon_m/\varepsilon_m A)_s} = 0 \tag{10}$$

$$\nabla \cdot (v\rho c_p T) - \nabla \cdot (\lambda \cdot \nabla T) + Q_{elec} + \frac{\sigma(T_s^4 - T_r^4)}{(1-\varepsilon_m/\varepsilon_m A)_s + 1/A_s F_{r,s} + (1-\varepsilon_m/\varepsilon_m A)_r} = 0 \tag{11}$$

where $Q_{elec} = (-\Delta H_{elec}) R_{elec} - P_{SOFC}$ is the local generated heat ($W\,m^{-2}$); $(-\Delta H_k)$ is the heat of reaction k; A is the area (m^2); $F_{r,s}$ is the gray-body transfer factor from the reformer surface to the solid oxide surface; σ is the Stefan–Boltzmann coefficient; ε_m is the emittance; P_{SOFC} is the local power density of the SOFC ($W\,m^{-2}$).

2.3. Calculation of thermal and electrical efficiencies

Base on the assumption that most of the generated hydrogen was combusted to supply heat for the steam reforming reaction, some heat generated was used as the heat source. The thermal efficiency, $Eff_{thermal}$, of an IIR-SOFC fuelled by different primary fuels was defined as the ratio between the heating value of hydrogen

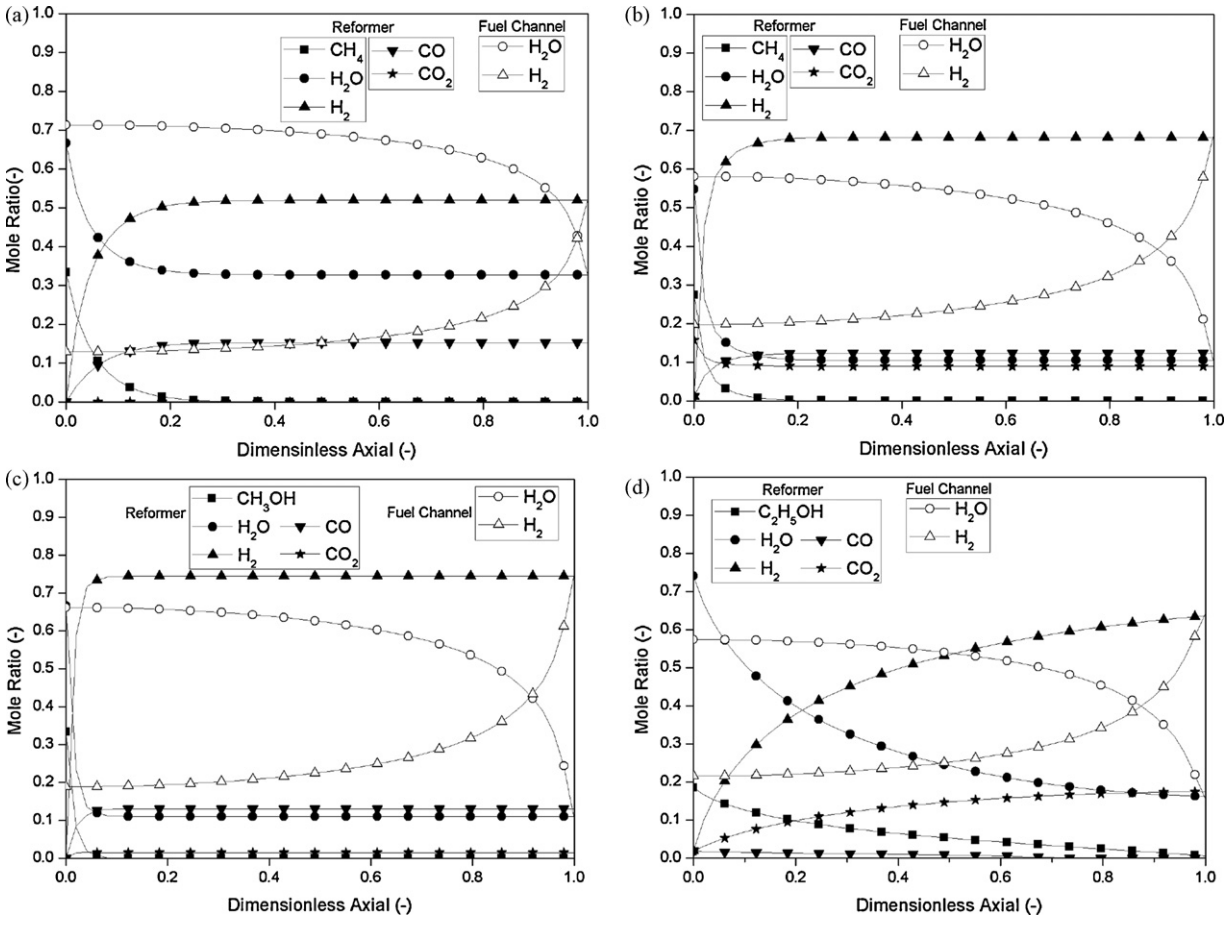

Fig. 3. Concentration profiles in reformer (black symbols) and fuel channel (white symbols) of IIR-SOFC fuelled by (a) methane, (b) biogas, (c) methanol and (d) ethanol (at base case conditions).

leftover from combustion with that of the inlet fuel, i.e.:

$$Eff_{thermal} = \frac{n_{H_2}^{out} LHV_{H_2,1173\ K} - \sum\left(-\Delta H_{reform}\right)}{\sum n_i^{in} LHV_{i,1173\ K}} \quad (12)$$

where n_i is number of moles for component i, and $LHV_{i,1173\,K}$ is the lower heating value of component i at 1173 K. In order to investigate the electrical efficiency, Eff_{elec}, outlet reformats were fed into SOFC and the electrical efficiency was defined as:

$$Eff_{elec} = \frac{P_{SOFC}.A_{act}}{\sum y_i^{in} LHV_{i,1173K}} \quad (13)$$

where A_{act} is the active area (m^2) and y_{fuel}^{in} is the mole fraction of the primary fuel.

3. Result and discussion

3.1. Thermodynamic property comparison

Before undertaking a thermodynamic analysis of an IIR-SOFC fuelled by different primary fuels, the thermodynamic properties of each fuel, i.e., methane, methanol, ethanol, and biogas (60% CH_4 and 40% CO_2) were identified in terms of lower heating value (LHV) and thermal efficiency. According to the thermal efficiency calculation, a steady-state operation was assumed and the inlet fuel was kinetically converted to hydrogen in the packed-bed reformer, which was eventually combusted to predict the thermal efficiency. It is noted that the simulation was carried out at 1173 K and 1 bar with the inlet steam to carbon (S/C) ratio of 2.0. Importantly, the limitation of gases transport through the packed catalyst was also

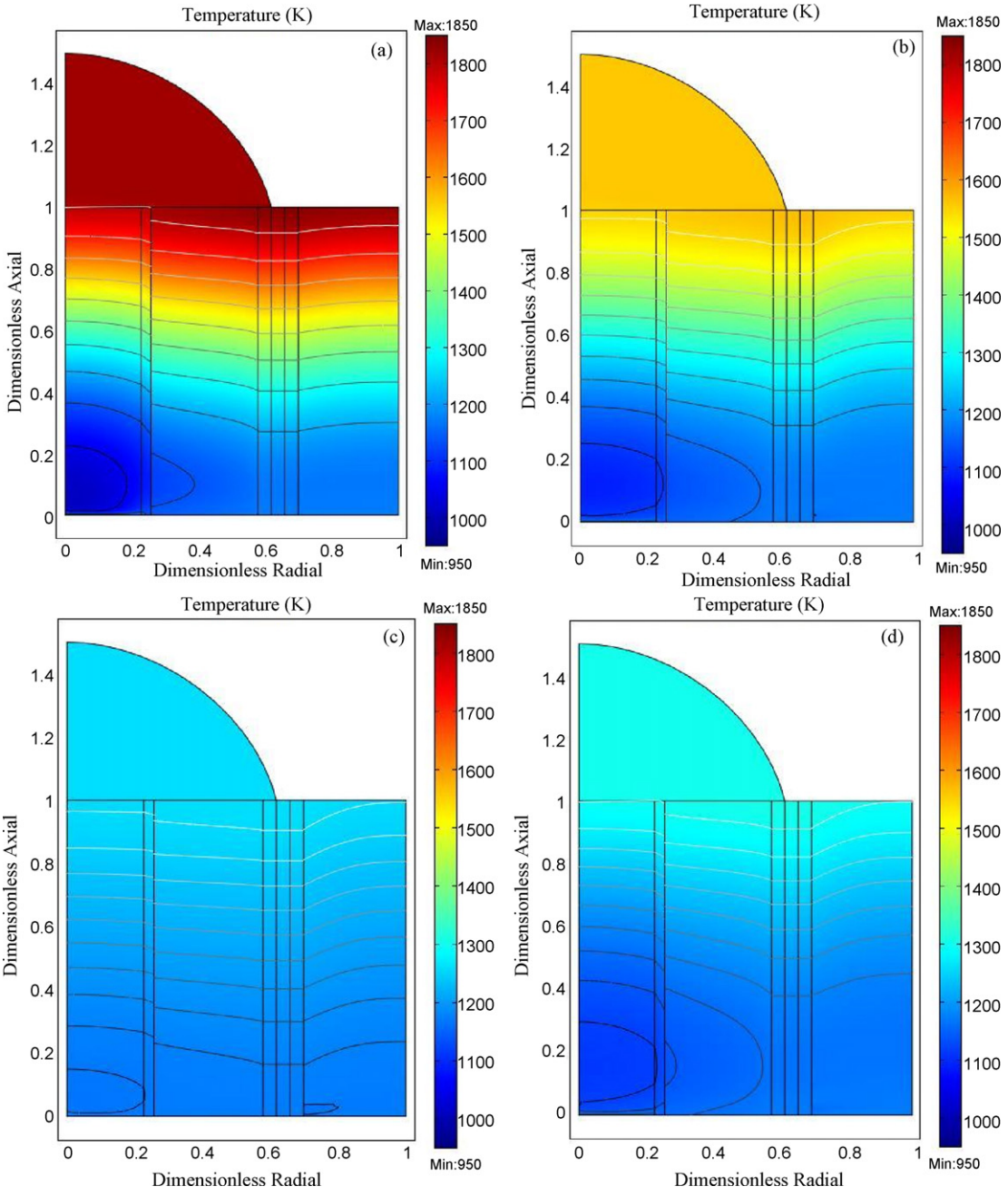

Fig. 4. Results from COMSOL® represented temperature gradients in reformer and fuel channel of IIR-SOFC fuelled by (a) methane, (b) biogas, (c) methanol and (d) ethanol (at base case conditions).

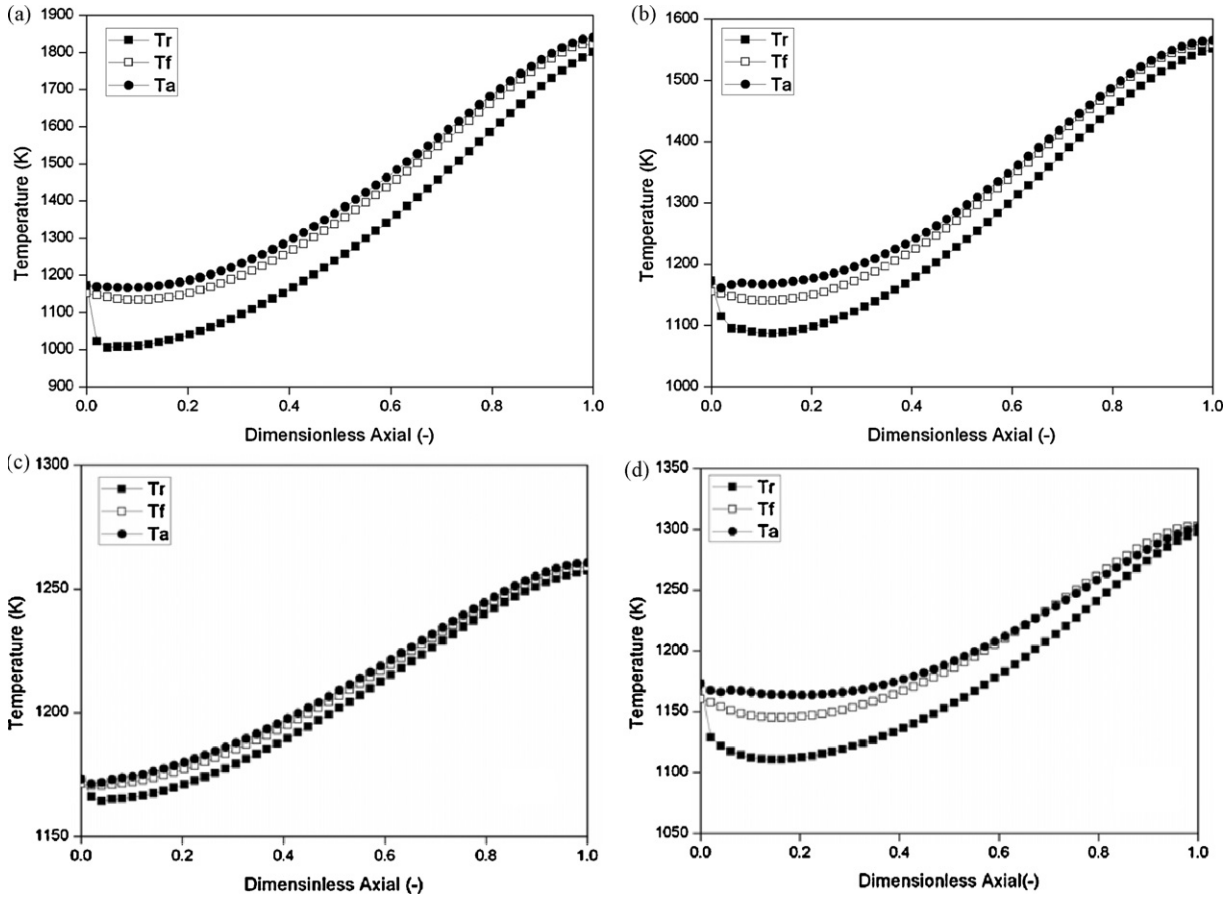

Fig. 5. Temperature profiles of reformer, fuel and air channels (T_r, T_f and T_a, respectively) for IIR-SOFC fuelled by (a) methane, (b) biogas, (c) methanol and (d) ethanol (at base case conditions).

taken into account. The dimensions of the system configuration are listed in Table 1, while the LHV and thermal efficiencies of each primary fuel are compared in Table 2. Among these primary fuels, alcohol-based fuels (methanol and ethanol) provide significantly higher thermal efficiency than methane-based fuels. Furthermore, the LHV of ethanol is considerably higher than those of other fuels, while that of methanol is close to that of methane. Hence, alcohol would be a promising candidate fuel for IIR-SOFC, IIR-SOFCs. The performance of an IIR-SOFC fuelled by these primary fuels in terms of electrical efficiency and temperature gradient along the system was then compared as presented in the following sections.

3.2. Modelling of IIR-SOFC fuelled by different fuels as based case

The non-isothermal model of IIR-SOFC was first simulated at 1 bar by introducing inlet fuels and steam at a S:C ratio of 2.0. A SOFC load voltage of 0.7 V and a fuel utilization of 80% were applied. Under these conditions, characteristic results, i.e., primary fuel conversion, product gas distribution and temperature gradient along the internal reformer and SOFC channels (both fuel and air channels) are shown in Figs. 3–5. The mole fraction profiles of primary fuels, hydrogen, steam, carbon monoxide, and carbon dioxide in reformer and fuel channel of SOFC, are presented in Fig. 3(a)–(d). Among these primary fuels, ethanol provides the slowest conversion rate along the reformer channel. At the outlet of the internal reformer, the product gas flows backward into fuel channel where hydrogen and carbon monoxide are electrochemically converted to steam and carbon dioxide.

Fig. 4(a)–(d) shows the results from COMSOL software representing temperature distributions in reformer, fuel and air channels for the IIR-SOFC system fuelled by different fuels, while Fig. 5(a)–(d) summarizes the temperature profiles in each channel. It can be seen that the heat generated from fuel cell side is sufficient for the internal reforming operation; nevertheless, a noticeable temperature gradient associated with indirect internal reforming operation is also observed for all types of fuel (as also reported by other researchers [4,6]). Among them, IIR-SOFC fuelled by methane shows the largest cooling spot at the first half of the reformer channel (reformer temperature decreases from 1173 to 1000 K), whereas IIR-SOFC fuelled by methanol presents the smoothest temperature profile (reformer temperature decreases from 1173 to 1163 K). It is noted that although the rate of the methanol conversion is faster than that of ethanol (Fig. 3(b) and (c)), the heat of the methanol steam reforming reaction is considerably lower, thus the temperature gradient for IIR-SOFC fuelled by methanol is smoother. The electrical efficiencies achieved from the IIR-SOFC with different fuels are compared in Table 3. It can be seen that methanol provides the greatest electrical efficiency; nevertheless, the system also requires the largest amount of inlet fuel compared with other fuels.

Table 3
Comparison of required volumetric flow rate and electrical efficiency achieved from IIR-SOFC fuelled different fuels.

Fuel	Properties	
	Volumetric flow rate	Electrical efficiency (%)
Methane	0.15	61.1
Biogas	0.18	46.7
Methanol	0.22	85.6
Ethanol	0.096	32.0

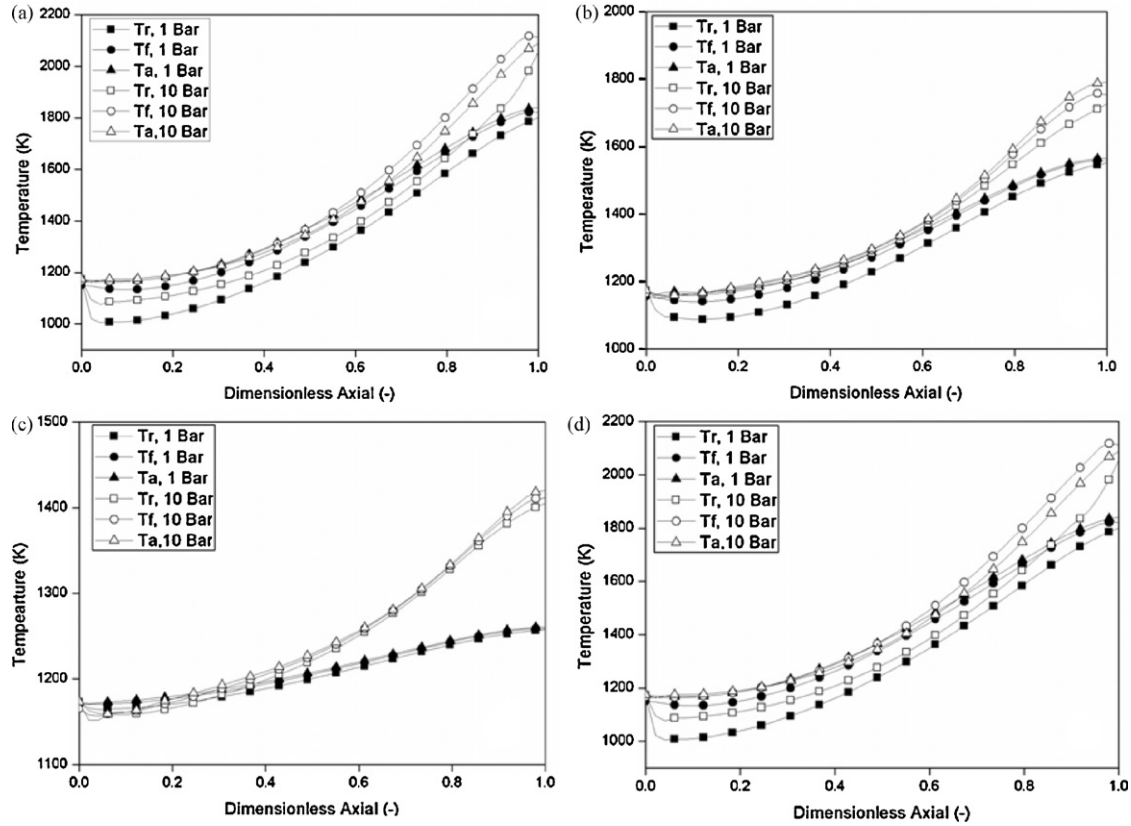

Fig. 6. Effect of operating pressure on temperature profile of IIR-SOFC fuelled by (a) methane, (b) biogas, (c) methanol and (d) ethanol.

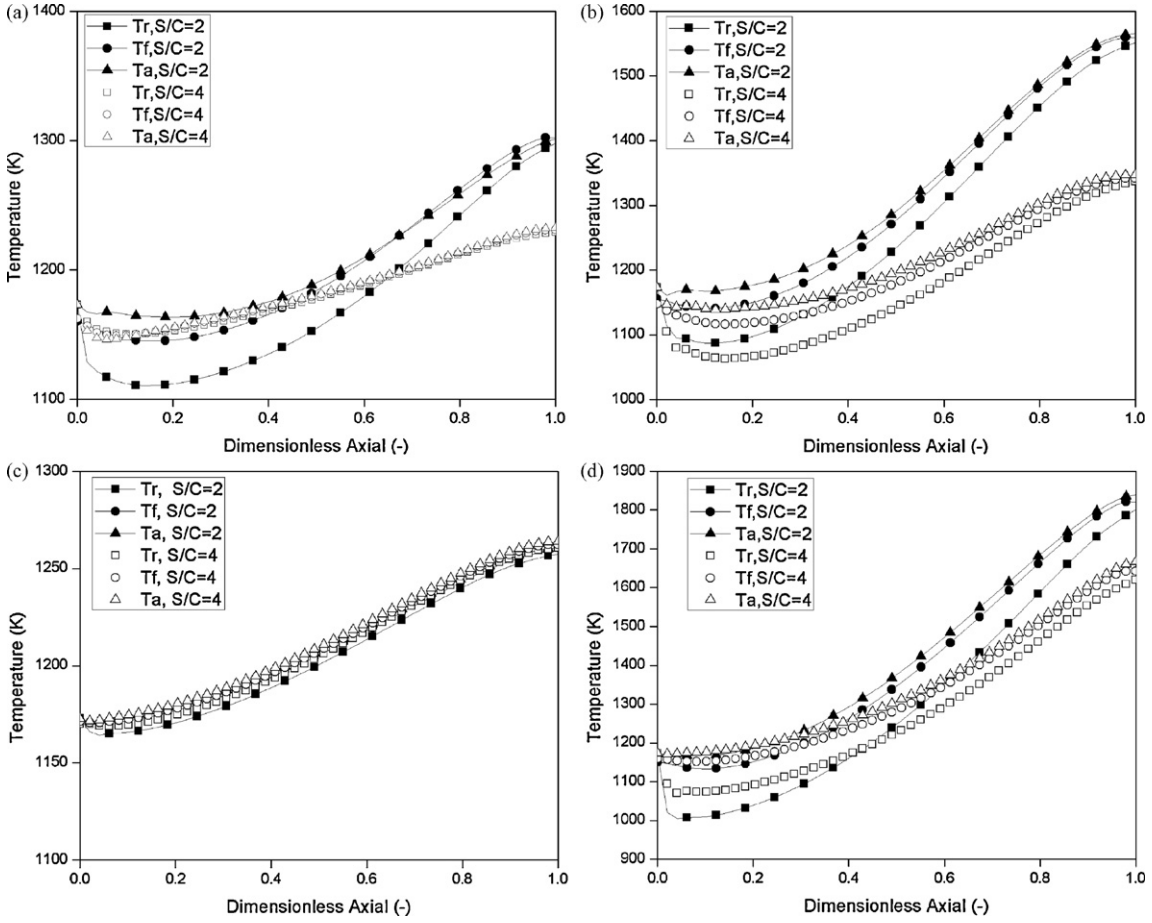

Fig. 7. Effect of S:C ratio on temperature profile of IIR-SOFC fuelled by (a) methane, (b) biogas, (c) methanol and (d) ethanol.

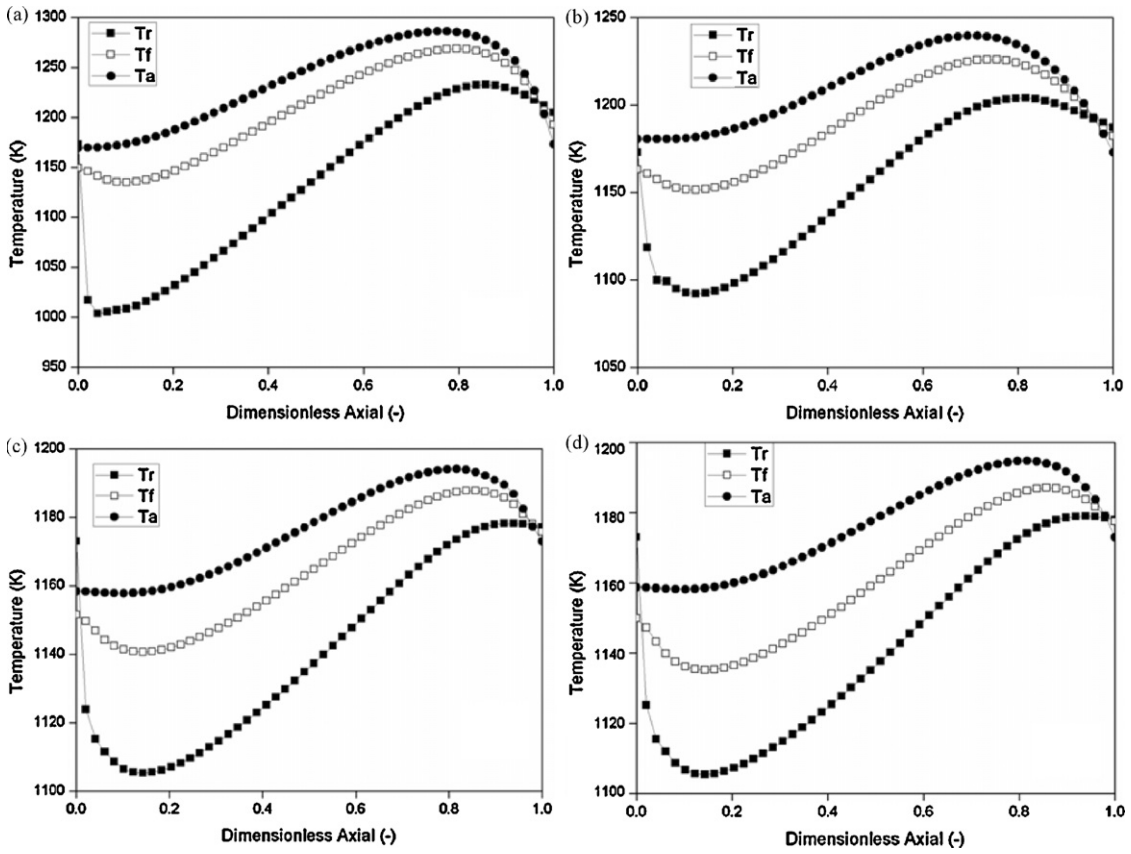

Fig. 8. Temperature profiles of reformer, fuel and air channels (T_r, T_f and T_a) for IIR-SOFC with co-flow pattern fuelled by (a) methane, (b) biogas, (c) methanol and (d) ethanol.

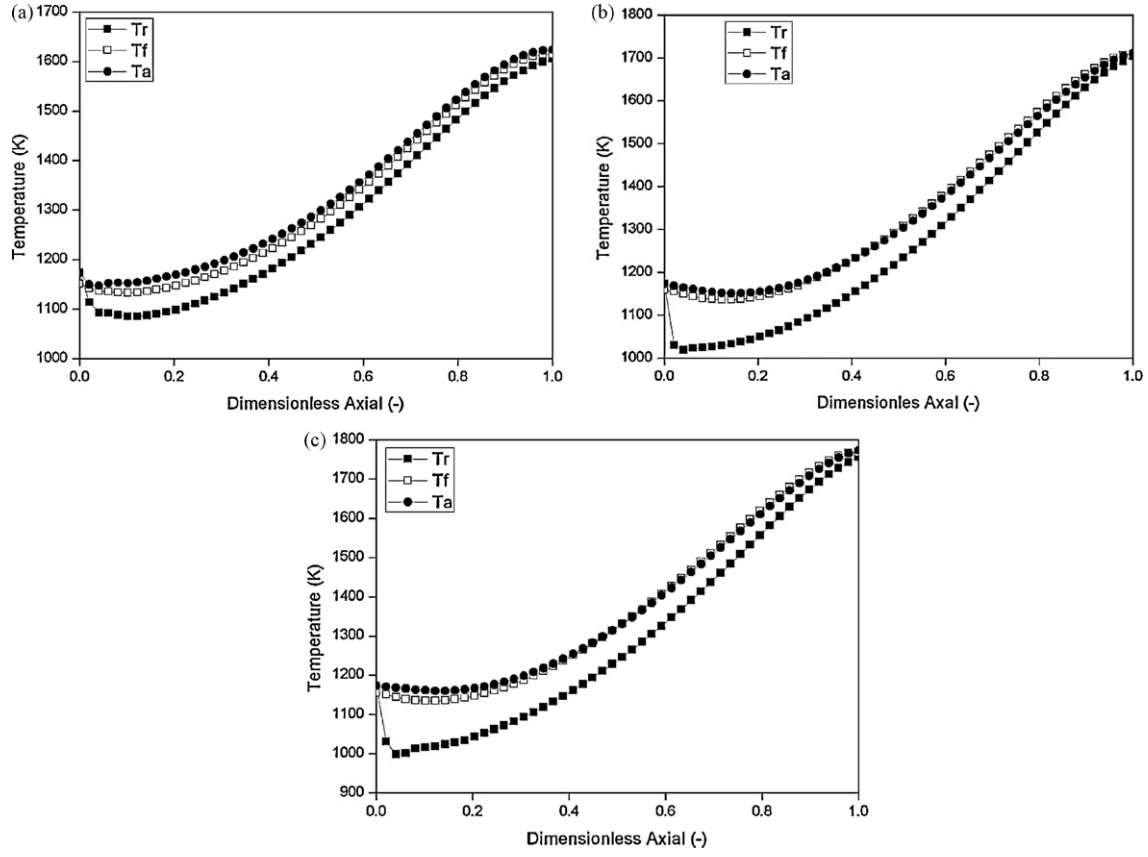

Fig. 9. Effect of CO_2 content in biogas ((a) 30%, (b) 20% and (c) 10%) on the temperature profiles of reformer, fuel and air channels (T_r, T_f and T_a) of IIR-SOFC system.

From the literature, the temperature gradient along the system can affect the cell performance and the properties of the ceramic component; the temperature difference along the SOFC system should be less than 10 K cm^{-1} [20]. According to the present analysis, only an IIR-SOFC fuelled with methanol can meet this criterion. Thus, as another aim of this study, several operating conditions, i.e., operating pressure, inlet S:C ratio and gas flow pattern are varied in order to minimize the temperature gradient as well as maximize the outputs (i.e., electrical efficiency) from an IIR-SOFC fuelled by these fuels.

3.3. Effect of pressure

According to the kinetic expressions for steam reforming of selected fuels, the operating pressure plays an important role on gas conversion behaviour as well as product selectivity. Thus, the effect of operating pressure on the system performance was determined by varying the operating pressure from 1 to 10 bar. As seen in Fig. 6(a)–(d), an increase in pressure significantly reduces the temperature drop at the entrance of reformer channel. This could be due to the effect of the partial pressure of gas species in the steam reforming and electrochemical reactions since the extent of the steam reforming rate reaction decreases with increasing pressure due to the thermodynamic restrictions and the kinetic expressions in use. It is also found that an increase of operating pressure results in a higher open-circuit potential and consequently lower polarization, which leads to higher electrical efficiency. According to simulation, the electrical efficiency of IIR-SOFC fuelled by methane, biogas, methanol and ethanol increases to 58.3, 44.8, 69.46, and 34.2%, respectively, when the operating pressure is increased from 1 to 10 bar. Thus, an increase in operating pressure is an effective way for reducing the temperature gradient, as well as enhancing cell performance.

3.4. Effect of steam to carbon (S/C) ratio

As the thermodynamic properties of inlet fluids are important factors that could influence the thermal behaviour of SOFC system, the effect of inlet steam content on the temperature gradient along the system and the system performance was investigated by varying the inlet steam to carbon (S:C) ratio from 2.0 to 4.0. Fig. 7(a)–(d) presents the effect of inlet S:C ratio on the temperature gradient along the reformer channel of an IIR-SOFC fuelled by different primary fuels. It can be seen that the cooling spot reduces when the ratio is increased for all types of fuel, particularly in the case of ethanol. This improvement could be caused by an increase in heat accumulated from excess steam fed into the system, which could be efficiently used for the endothermic steam reforming reaction. Nevertheless, it is also found that the electrical efficiency considerably decreases with increasing inlet S:C ratio (decreases to 33.3, 29.3, 54.6 and 15.4% for IIR-SOFC fuelled by methane, biogas, methanol and ethanol, respectively, when the inlet S:C ratio increases from 2.0 to 4.0). The decrease could be due to the higher cell polarization with increasing inlet S:C ratio and the higher energy requirement to vaporize steam when excess steam is introduced to the system [20].

3.5. Effect of flow direction

For typical autothermal application, e.g., a heat exchanging system, the flow direction of exchanged fluids strongly affects the heat transfer and reaction behaviour in the fluid stream; thus the effect of the fuel and oxidant flow direction on the IIR-SOFC performance was also considered in the present work. In previous sections, air flow is counter-flow to fuel flow in the fuel channel of SOFC (a so-called 'counter-flow' pattern). Alternatively, fuel and air streams can be passed in the same direction, a so-called "co-flow" pattern. The system behaviour of with co-flow pattern was analyzed by changing mass and energy balances in the air channel along with their corresponding boundary conditions, while keeping all other operating conditions identical to those of the counter-flow pattern. Fig. 8(a)–(d) shows the temperature profiles along all channels of an IIR-SOFC with co-flow pattern. Compared with the data in Fig. 5, it can be seen that the flow direction of fuel gases and air strongly affects the temperature gradient along the system. The IIR-SOFC with a co-flow pattern provides smoother temperature distribution with a higher average cell temperature, which leads to a reduction in cell overpotentials and consequently yields a higher electrical efficiency (increases to 55.8, 46.6, 67.1 and 39.8% for methane, biogas, methanol and ethanol, respectively). The high efficiency of an IIR-SOFC with a co-flow pattern is due to the good matching between the heat exothermically supplied from electrochemical reaction and the heat required for endothermic steam reforming along the SOFC system, thus it is concluded that an IIR-SOFC with co-flow pattern is more satisfactory than that with counter-flow pattern.

3.6. Effect of CO_2 content in biogas

According to the above study, the electrical efficiency of IIR-SOFC fuelled by biogas is relatively low due to the high content of CO_2 in biogas. It is well known that the presence of a high CO_2 content is a major problem with biogas in terms of several energy aspects, e.g., combust for power generation or compress and use as fuel in vehicle; thus the removal of CO_2 from biogas, which can be done by means of several techniques, e.g., water scrubbing, pressure swing adsorption or membrane technology, has been proposed and widely applied recently. In the present work, the effect of CO_2 content in biogas on system performance was also studied by varying the CO_2 content from 40 to 30, 20 and 10%. It is found that the electrical efficiency increases with decreasing CO_2 content (from 34.5 to 35.9, 38.2 and 39.2%, respectively); nevertheless, it can be seen from Fig. 9(a)–(c) that the content of CO_2 also affects the temperature gradient along the system. The temperature difference increases from 28.1 to 30.4, 42.8 and 47.6 K cm^{-1} when the CO_2 content is decreased from 40 to 30, 20 and 10%, respectively, thus it could affect the ceramic component of the SOFC and result in mechanical failure due to thermally induced stresses.

4. Conclusions

The simulation indicates that, among the four types of fuel studied, an IIR-SOFC fuelled by methanol provides the greatest performance in terms of electrical efficiency and temperature gradient along the system. It is also found that the content of CO_2 in biogas strongly affects the system performance; by removal of some CO_2 from biogas, the electrical efficiency can be improved but a larger temperature gradient is expected. By increasing the operating pressure, the system efficiency increases and the temperature gradient can be minimized. The use of a high inlet S:C ratio can reduce the cooling spot at the entrance of the internal reformer channel but the electrical efficiency considerably decreases due to the higher cell polarization and higher energy requirement to vaporize steam when excess steam is introduced to the system. An IIR-SOFC with a counter-flow pattern is also compared with an IIR-SOFC that has a co-flow pattern. It is found that a co-flow pattern provides higher voltage a and smoother temperature gradient along the system due to better matching between the heat supplied from the electrochemical reaction and the heat required for the steam reforming reaction.

Acknowledgements

The financial support from the Thailand Research Fund (TRF) and Commission on Higher Education, and the Thailand Graduate Institute of Science and Technology (TGIST) program, Thailand's National Science and Technology Development Agency (NSTDA), grant no. TG-55-20-50-058D throughout this project is gratefully acknowledged.

References

[1] G. Hoogers (Ed.), Fuel Cell Technology, 1st edition, 2003.
[2] P. Dokamaingam, S. Assabumrungrat, A. Soottitantawat, I. Sramala, N. Laosiripojana, Int. J. Hydrogen Energy 34 (2009) 410–421.
[3] H.-K. Park, Y.-R. Lee, M.-H. Kim, G.-Y. Chung, S.-W. Nam, S.-A. Hong, T.-H. Lim, H.-C. Lim, J. Power Sources 104 (2002) 140–147.
[4] P. Aguiar, D. Chadwick, L. Kershenbaum, Chem. Eng. Sci. 57 (2002) 1665–1677.
[5] K. Eguchi, Handbook of Fuel Cells 4 (2003) 1057–1069.
[6] D. Sánchez, R. Chacartegui, A. Munoz, T. Sánchez, J. Power Sources 60 (2006) 1074–1087.
[7] J. Xu, G.F. Froment, AIChE J. 35 (1989) 88–96.
[8] B.A. Peppley, J.C. Amphlett, L.M. Kearns, R.F. Mann, Appl. Catal. A: Gen. 179 (1999) 31–49.
[9] M.E.E. Abashar, Int. J. Hydrogen Energy 29 (2004) 799–808.
[10] D.R. Sahoo, S. Vajpai, S.P.K. Pant, Chem. Eng. Sci. 125 (2007) 139–147.
[11] R. Mauri, J. Eng. Math. 33 (1998) 103–112.
[12] B. Todd, J.B. Young, J. Power Sources 110 (2002) 186–200.
[13] E.N. Fuller, P.D. Schettler, J.C. Giddings, Ind. Eng. Chem. 58 (1966) 19–27.
[14] R. Suwanwarangkul, E. Croiset, M.W. Fowler, P.L. Douglas, E. Entche, M.A. Douglas, J. Power Sources 122 (2003) 9–18.
[15] H. Zhu, R. Kee, V. Janardhanan, O. Deutschmann, D. Goodwin, J. Electrochem. Soc. 152 (2005) A2427–A2440.
[16] H. Zhu, A.M. Colclasure, R.J. Kee, Y. Lin, S.A. Barnett, J. Power Sources 161 (2006) 413–419.
[17] Y. Matsuzaki, I. Yasuda, Solid State Ionics 126 (1999) 307–313.
[18] Y. Lin, Z. Zhan, S.A. Barnett, J. Power Sources 158 (2006) 1313–1316.
[19] D.L. Damm, A.G. Fedorov, J. Power Sources 143 (1–2) (2005) 158–1653.
[20] A.E. Lutz, R.W. Bradshaw, J.O. Keller, D.E. Witmer, Int. J. Hydrogen Energy 28 (2003) 159–167.